Effects of thin film Pd deposition on the hydrogen permeability of Pd60Cu40 wt% alloy membranes

Al-Mufachi, Naser; Nayebossadri, S.; Speight, John; Bujalski, W.; Steinberger-wilckens, R.; Book, D.

DOI:
10.1016/j.memsci.2015.07.015

Journal of Membrane Science 493 (2015) 580–588

Contents lists available at ScienceDirect

Journal of Membrane Science

journal homepage: www.elsevier.com/locate/memsci

Effects of thin film Pd deposition on the hydrogen permeability of $Pd_{60}Cu_{40}$ wt% alloy membranes

N.A. Al-Mufachi [a,*], S. Nayebossadri [b], J.D. Speight [b], W. Bujalski [a,1], R. Steinberger-Wilckens [a], D. Book [b]

[a] Centre for Hydrogen and Fuel Cell Research, School of Chemical Engineering, University of Birmingham, Edgbaston B15 2TT, UK
[b] School of Metallurgy and Materials, University of Birmingham, Edgbaston, Birmingham B15 2TT, UK

ARTICLE INFO

Article history:
Received 18 July 2014
Accepted 4 October 2014
Available online 13 July 2015

Keywords:
Pd–Cu membrane
Dense metal membrane
Pd thin film
Hydrogen separation
Interdiffusion

ABSTRACT

$Pd_{60}Cu_{40}$ wt% ($Pd_{47.3}Cu_{52.7}$ at%) membranes were surface modified by depositing Pd thin films of three different thicknesses (~100, 800 and 1400 nm) on to one side of a range of as-received $Pd_{60}Cu_{40}$ wt% cold-rolled foils via magnetron sputtering. The hydrogen permeability of the membranes was then measured and compared to the uncoated material. The $Pd_{60}Cu_{40}$ wt% membrane coated with a 1400 nm thick Pd thin film positioned on the feed side (445 kPa of hydrogen pressure) during hydrogen permeability measurements and cycled between 50 and 450 °C achieved the highest hydrogen permeability of 1.09×10^{-8} mol m^{-1} s^{-1} $Pa^{-0.5}$ at 450 °C in the third cycle. This is a 58% increase on the value measured for the as-received $Pd_{60}Cu_{40}$ wt% membrane under the same conditions.

This improvement can be attributed to a Pd-rich Pd–Cu face centred cubic (FCC) phase forming through interdiffusion between the Pd thin film and bulk Pd–Cu membrane as a result of the test conditions used during hydrogen permeability measurements. This introduces a larger hydrogen concentration gradient across the membrane due to the relatively high hydrogen solubility of the Pd-rich Pd–Cu FCC phase resulting in the observed increase in permeability.

The $Pd_{60}Cu_{40}$ wt% membranes coated with a ~1400 nm and ~800 nm thick Pd thin film retained an almost pure Pd surface throughout cycling between 50 and 450 °C with a feed and permeate hydrogen pressure of 445 and 100 kPa, respectively. For the deposition technique and test conditions used throughout this work, these surface modified Pd–Cu membranes appear to stabilise the Pd thin films upon cycling across the critical temperature of 295 °C.

1. Introduction

Currently, most of the commercially available hydrogen gas is produced via steam methane reforming [1]. However, with the expected growth in the proton exchange membrane fuel cell industry it is anticipated that there will also be a growing need for ultra-pure hydrogen of grade 5.0 (99.999%) [2,3]. Palladium-based dense alloy membranes, such as Pd–Ag and Pd–Cu, are used for hydrogen purification applications due to their high catalytic activity for hydrogen dissociation, high hydrogen permeability and mechanical robustness [4–6]. The Pd–Cu alloy system is of particular interest as the lower Pd content may reduce the cost and the Pd-rich Pd–Cu FCC phase exhibits better resistance to H_2S poisoning in comparison to other commercially available membranes such as Pd–Ag alloys [7–12].

According to the Pd–Cu phase diagram (Fig. 1), the $Pd_{60}Cu_{40}$ wt% composition contains a CsCl-type ordered body centred cubic (BCC) phase below 450 °C [13]; this has been reported [4,7,8,12,14,15] to possess the highest hydrogen permeability within this binary alloy system. Deviation from this optimum composition by 3 wt% or more can result in at least a 50% reduction in hydrogen permeability [16]. Hence, the BCC $Pd_{60}Cu_{40}$ wt% alloy membranes have been selected for this study and any further reference to Pd–Cu membranes in this work will be of this composition unless otherwise stated.

In the Pd–Cu system, diffusivity of hydrogen in the BCC phase is two orders of magnitude greater than in the FCC phase [14,15,18,19]. At the $Pd_{60}Cu_{40}$ wt% composition, above 450 °C the disordered FCC phase begins to form and at temperatures higher than 600 °C only this phase exists. The Pd-rich Pd–Cu FCC phase with the composition $Pd_{100-x}Cu_x$ wt% ($0 \leq x \leq 20$) has relatively high hydrogen solubility [20–22] and an enhanced resistance to H_2S contamination over the BCC phase [10,12]. Modifying the

* Corresponding author.
E-mail address: naser.al-mufachi@hotmail.co.uk (N.A. Al-Mufachi).
[1] Deceased 30 Jan, 2013

http://dx.doi.org/10.1016/j.memsci.2015.07.015

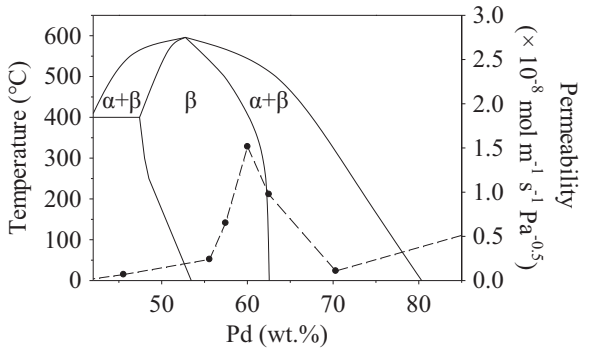

Fig. 1. Pd–Cu phase diagram where 'α' denotes the FCC phase and 'β' denotes the BCC phase. The phase diagram has been reproduced from literature [13,17] and also features a hydrogen permeability dashed line plot as a function of Pd content at 350 °C compiled using data from Howard et al. [15].

surface composition of a $Pd_{60}Cu_{40}$ wt% membrane through the deposition of Pd may introduce a Pd-rich Pd–Cu FCC layer that may potentially improve hydrogen permeability and H_2S resistance of the membrane.

The aim of this work is to explore the possibility of creating a Pd-rich Pd–Cu FCC phase on the surface of a BCC $Pd_{60}Cu_{40}$ wt% membrane that is stable under typical operating conditions to determine the effects on hydrogen permeability. This can be achieved by depositing a Pd thin film onto one side of a $Pd_{60}Cu_{40}$ wt% membrane using magnetron sputtering. Annealing the surface modified membrane creates a Pd-rich layer containing the FCC phase produced via Cu interdiffusion out of the bulk $Pd_{60}Cu_{40}$ wt% membrane and into the Pd thin film.

Pure Pd membranes also undergo a phase transformation during thermal cycling in a hydrogen atmosphere which leads to rupturing when the critical temperature of 295 °C is passed at hydrogen pressures below 2 MPa [4]. The Pd–Cu alloy avoids this at the cost of a lower hydrogen surface absorption. Coating the Pd–Cu membranes with a pure Pd surface could lead to enhanced surface absorption of hydrogen whilst retaining the mechanical robustness of the alloy membrane.

Successful manipulation of the $Pd_{60}Cu_{40}$ wt% alloy surface composition could have the potential to produce a membrane with enhanced properties competitive with the more popular and expensive Pd–Y and Pd–Ag alloy systems.

2. Experimental

2.1. Sample preparation

Cold rolled $Pd_{60}Cu_{40}$ wt% foil was supplied by Johnson Matthey Noble Metals (Royston, UK) with an approximate thickness of 31.3 ± 0.8 μm. Seven 21 mm diameter circular disc membranes and three square ($\sim 5 \times 5$ mm) foil offcuts were cut from the same as-received Pd–Cu foil batch and cleaned in acetone for 5 min using an ultrasonic bath. In addition, a 67.8 ± 1.8 μm thick Pd (99.95%) cold rolled foil, supplied by Goodfellow, was used during this work acting as a standard.

2.2. Magnetron sputtering

A thin Pd film was deposited using a closed field unbalanced magnetron sputter ion plating (CFUBMSIP) system produced by Teer Coatings Ltd. [23]. The circular $Pd_{60}Cu_{40}$ wt% foil membranes were mounted inside the sputtering system, evacuated to 10^{-7} kPa and subjected to an ion cleaning process with Ar plasma prior to sputtering. A Pd target (99.9% purity) was used to sputter Pd–Cu on to the membranes at a target current of 1 A and Ar flux of 25 standard cubic centimetres per minute. Three different coating times were chosen in order to produce Pd–Cu membranes with varying Pd thin film thicknesses on one side.

Table 1
Summary of samples investigated in this work.

	Pd coating time (s)	Pd thin film thickness (nm)
Membrane A	Not coated	–
Membrane B and Foil B	50	~100
Membrane C and Foil C	1000	~800
Membrane D and Foil D	1800	~1400

The Pd–Cu membranes are categorised into four types as shown in Table 1. Membrane A was not Pd sputter coated and remained in the as-received state. Membranes B, C and D denote a Pd–Cu membrane that has been Pd sputter coated for 50, 1000 and 1800 s, respectively.

A Pd–Cu foil offcut was Pd sputter coated alongside Membrane B, Membrane C and Membrane D to create Foil B, Foil C and Foil D, respectively. In addition, a glass slide was Pd sputter coated with each membrane type whereby a section of the glass surface was protected with Kapton tape. Removal of the tape revealed the uncoated surface of the glass slide creating a step from which the Pd film thickness could be measured. Profilometry was used to accurately measure the Pd film thickness using an Ambios XP-200 Stylus surface profilometer with a scanning speed of 0.1 mm s^{-1} using a 2 mg tip force. The Pd thin film thickness for each membrane type is shown in Table 1 based on the profilometry measurements performed on the respective Pd coated glass slides.

2.3. Hydrogen permeability measurement

A bespoke membrane permeability rig (MPR) was used to measure the hydrogen permeability of the Pd membrane in addition to Membranes A–D. Each membrane is secured in a sample holder which maintains a hermetic seal within an Inconel reactor. A Pfeiffer TSU-071E turbo-molecular drag pumping station with a membrane backing pump is used to evacuate the reactor down to $\sim 10^{-6}$ kPa. A Brookes 5850S Mass Flow Controller (MFC) is used to control the gas inlet to the feed side of the sealed membrane. To prevent any build-up of contaminants and to maintain a stable hydrogen feed pressure, the feed gas is allowed to flow continuously and is bled through a second MFC. An additional MFC was utilised to monitor the quantity of hydrogen that permeates through the membrane.

The temperature of the membrane was controlled using an Elite Thermal Systems Ltd. split furnace and monitored using Inconel K-type thermocouples. All MFCs and the split furnace are controlled using a PC and SpecView data logging software.

The experimental details are summarised in Table 2. All membranes were heated at a ramp rate of 2 °C min^{-1} and then furnace cooled at a cooling rate of approximately 0.5 °C min^{-1}.

The seven membranes were tested in the MPR positioned on top of a porous stainless steel support. A hydrogen feed pressure of 445 kPa and permeate pressure of 100 kPa were applied to all membranes. Membrane A, Membrane B-F, Membrane B-P, Membrane C-F, Membrane C-P, Membrane D-F and Membrane D-P were cycled three times between 50 and 450 °C. The suffix '-F' indicates that the Pd thin film deposited on Membranes B–D were positioned on the feed side during MPR testing. The '-P' indicates that the Pd thin film deposited on Membranes B–D were positioned on the permeate side during MPR testing.

Subsequent to Membrane A completing three cycles between

Table 2
Experimental summary.

	Notes
Membrane A	
Membrane A*	* Indicates membrane permeability data acquired during the third cycle between 250 and 450 °C after completing two cycles between 250 and 700 °C
Membrane B-F	Pd thin film positioned on the feed side
Membrane B-P	Pd thin film positioned on the permeate side
Membrane C-F	Pd thin film positioned on the feed side
Membrane C-P	Pd thin film positioned on the permeate side
Membrane D-F	Pd thin film positioned on the feed side
Membrane D-P	Pd thin film positioned on the permeate side

50 and 450 °C, two cycles were performed between 250 and 700 °C in order to homogenise the membrane. The '*' denotes hydrogen permeability measurements acquired for Membrane A between 250 and 450 °C following the cycles between 250 and 700 °C.

2.4. X-ray diffraction analysis

Ex-situ X-ray diffraction (XRD) patterns were acquired for both the top and basal surfaces of the membranes before and after MPR testing for phase identification, to observe any phase transformations as a result of MPR testing and to determine phase composition. XRD analysis was performed under ambient conditions. Depending on the X-ray penetration depth, the XRD patterns will contain information related to both the Pd thin film in Membranes B–D, as well as the underlying Pd–Cu membrane. The XRD analyses were performed with a Bruker D8-Advance diffractometer using monochromatic $CuK_{\alpha 1}$ radiation ($\lambda = 1.54056$ Å) providing an approximate penetration depth of 2 μm.

2.5. Scanning electron microscopy/energy dispersive spectroscopy analysis

Scanning electron microscopy (SEM) and energy dispersive spectroscopy (EDS) were performed in secondary electron imaging mode using a Jeol 6060 microscope. The microscope is equipped with INCA EDAX software. This was used to determine the composition of the as-received foil and any compositional variation in the membranes before and after MPR testing.

2.6. X-ray photoelectron spectroscopy

X-ray photoelectron spectroscopy (XPS) depth profiling of the as-deposited Foils B, C and D was performed in order to investigate any interdiffusion occurring between the Pd thin film and bulk Pd–Cu foil during the sputtering process. In addition, XPS depth profiling was performed on Membranes B-F, B-P, C-F, C-P, D-F and D-P following MPR testing in order to examine the effects of elevated temperatures and hydrogen pressures on near surface composition. A 25 nm etch cycle was used on Foil B to achieve high resolution of the relatively smaller interdiffusion region whereas an etch cycle of 50 nm was employed for Foils C and D.

A Thermo K-Alpha XPS Spectrometer with a monochromated K-Alpha source fitted with a MAGCIS ion gun was used for the depth profile analysis. The charge compensation was on during measurements. A monatomic Ar gun mode was used to perform the etch cycles with a 2 keV ion beam. The scan area was 2×2 mm and a reference etching rate of 0.21 nm s^{-1} based on a Ta_2O_5 standard was implemented to estimate the etch depth. An appropriate etch cycle and etch depth was selected according to the Pd thin film thickness being analysed. Thinner Pd films had a shorter etch cycle compared to relatively thicker Pd films in order to achieve higher resolutions of the interface region.

3. Results and discussion

3.1. Pre-MPR membrane characterisation

To accurately determine the composition of the as-received Pd–Cu foil, Vegard's law [24] (Eq. (1)) was used. This is an empirical rule that stipulates a linear correlation between crystal lattice parameter (a) and the alloy concentration of the constituent elements. It should be noted that positive and negative deviations from this principle can occur; however, in this work it is assumed that compositions determined using Vegard's law are a good approximation. Literature data [25–38] was used to compile a plot of FCC Pd–Cu lattice parameters as a function of Pd concentration (Fig. 2).

Eq. 1 was determined from a line of best fit of the Fig. 2 data where x_{Pd} is the Pd concentration given in at%.

$$a = (2.75 \times 10^{-3}) x_{Pd} + 3.62 \quad (1)$$

The FCC lattice parameter of Membrane A was determined using XRD data analysis giving an average of 3.757 ± 0.003 Å that is comparable to published values of the same alloy composition which range from 3.75 to 3.763 Å [39–43]. Using Eq. (1), it was calculated that Membrane A had an average FCC phase composition of $Pd_{48.6 \pm 0.9}Cu_{51.4 \pm 0.9}$ at% which corresponds to $Pd_{61.3 \pm 0.9}Cu_{38.7 \pm 0.9}$ wt%. EDS results provided a similar average phase composition of $Pd_{59.2 \pm 0.8}Cu_{40.8 \pm 0.8}$ wt%.

XRD analysis of Membranes A–D (Fig. 3) showed the presence of the FCC crystal structure which is the result of quenching the alloy from the high temperature FCC phase during the melting process. The Pd thin film in Membranes B–D is indicated by the Pd diffraction peaks. The XRD patterns for Membranes C and D show relatively high intensity in the Pd(111) diffraction peaks and high Pd(111)/Pd(200) peak intensity ratios demonstrating that with prolonged coating times the Pd adatoms exhibit a preference for occupying the (111) plane which is the most densely packed plane of the FCC crystal structure.

Fig. 4 shows the XPS depth profile plots obtained for Foils B, C and D in the as-deposited state which are representative of Membranes B, C and D, respectively. It should be noted that the film thickness measured for the Pd coated glass slides is considered more accurate as the Pd thin film did not undergo

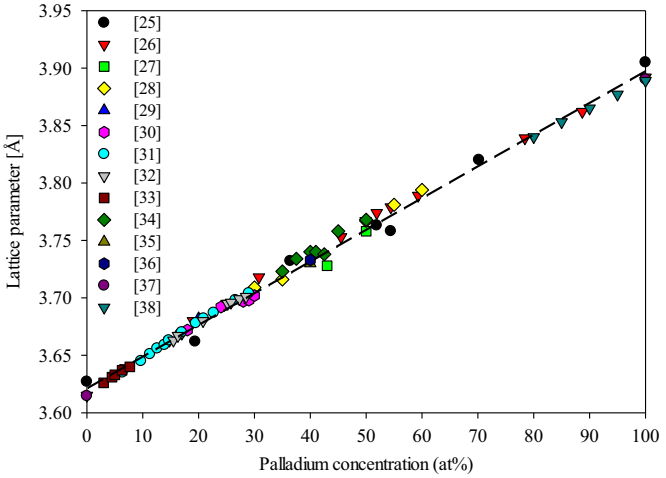

Fig. 2. FCC Pd–Cu alloy lattice parameter as a function of Pd content featuring a dashed line of best fit.

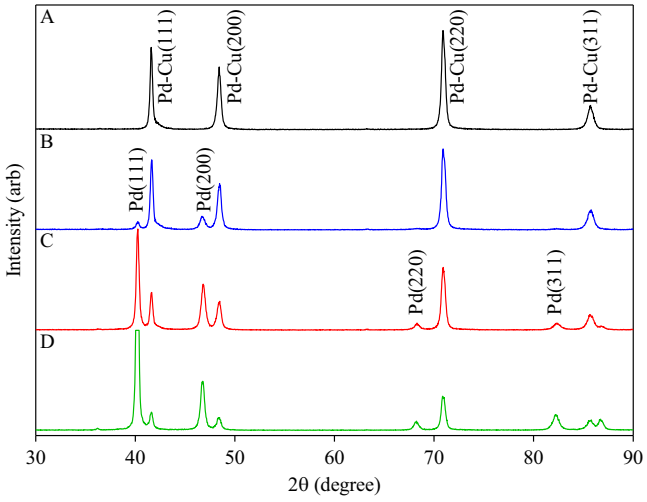

Fig. 3. XRD patterns acquired for Membrane A and the Pd sputter coated surfaces of Membranes B–D in the as-deposited state prior to MPR testing which indicate a single phase FCC crystal structure present in the bulk Pd–Cu membranes. The FCC Pd diffraction peaks shown in patterns B, C and D indicate the presence of the Pd thin film in Membranes B, C and D, respectively.

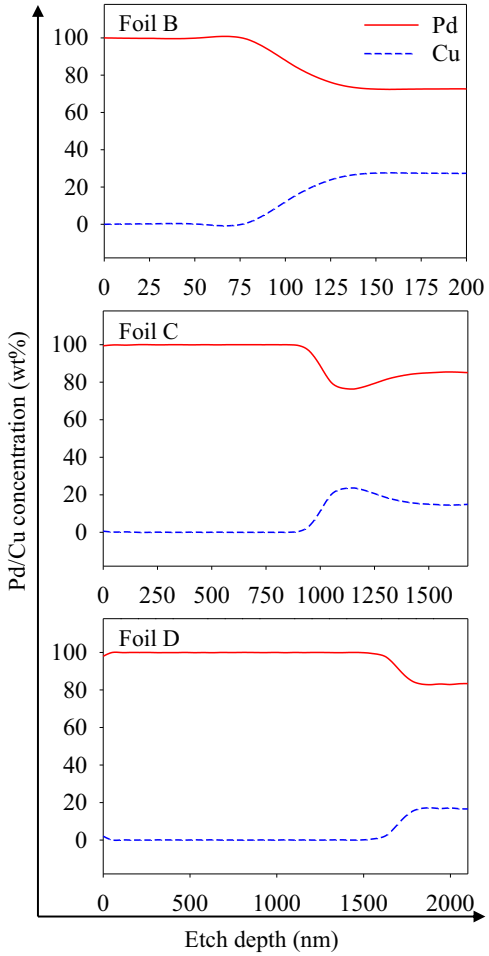

Fig. 4. XPS depth profile analysis of Foils B–D in the as-deposited state.

interdiffusion with the glass slide. Film thickness determined using XPS is considered less reliable since the etching rate is based on a Ta_2O_5 standard. In addition, the Pd thin films had experienced interdiffusion with the bulk Pd–Cu foil during deposition. This made it unclear where the Pd thin film ends and the bulk Pd–Cu foil starts. Smaller etch cycles would be necessary in order to more accurately measure the extent of the interdiffusion region.

For Foil B, the top 75 nm of the thin film is pure Pd below which an interdiffusion region exists. Note that the XPS depth profile is performed down to a depth of 200 nm and it may be possible that the interdiffusion region may continue beyond this point. This is clear evidence that interdiffusion between the deposited Pd thin film and bulk Pd–Cu foil occurs during the sputtering process. Significant interdiffusion can occur between bimetallic interfaces in bulk metals and alloys at the Tammann temperature [44]. This is defined as half of the melting point in Kelvin (K) of the constituent metals hence the Tammann temperature for the Pd–Cu system ranges between 679 K (326 °C) for Cu and 914 K (641 °C) for Pd. Therefore, it is expected that Cu atoms will be more mobile than Pd atoms during the interdiffusion process.

Various works on this topic [45–50] have shown that significant interdiffusion can occur in Pd–Cu thin films fabricated using deposition techniques such as electrodeposition, thermal evaporation and magnetron sputtering. Bukaluk [50] reports interdiffusion between Pd/Cu multilayers occurring at temperatures as low as 120 °C. The authors have attributed this phenomenon to the polycrystalline nature of the deposited thin films, which introduce grain boundary defects capable of promoting interdiffusion.

It may seem unlikely that either Membrane B or Foil B could reach the necessary temperatures for interdiffusion to occur in just 50 s of Pd deposition. However, it should be noted that irrespective of the short deposition time, it is possible for the Pd atoms to arrive at the surface of the Pd–Cu foil with sufficient kinetic energy for interdiffusion to take place as evidenced in Fig. 4.

For Foil C, the Cu concentration begins to rise at an approximate depth of 890 nm and plateau at 1050 nm indicating the interdiffusion region and providing further proof that interdiffusion occurs during Pd deposition. Deeper into Foil C, a region resembling a bottleneck exists originating from the bulk Pd–Cu foil showing the Cu concentration decreasing to form a second plateau at a depth of 1500 nm. This could be caused from the residual effects of coring brought about by the quenching of the Pd–Cu alloy during the melting process. As a consequence, the relatively lower melting point Cu atoms diffuse towards the extremities of the foil and the Pd atoms concentrate towards the inner region. The total analysis depth is approximately 1680 nm although it may be necessary to analyse to greater depths in order to reach the original composition of the underlying Pd–Cu foil ($\sim Pd_{60}Cu_{40}$ wt%).

It is apparent in Foil D, that the Cu concentration begins to increase at an approximate depth of 1520 nm indicating the start of the interdiffusion region and plateaus at around 1800 nm. Also, it would seem necessary to continue analysis to greater depths in order to reach the end of the interdiffusion region. Following Pd deposition, Foils C and D had undergone heating during the Pd deposition process and it was necessary for the foils to cool sufficiently prior to handling.

3.2. MPR results

Fig. 5 displays a plot of hydrogen permeability as a function of temperature comparing the third cycle completed by each membrane studied in this work. However, the Membrane A* curve represents the third cycle completed between 250 and 450 °C subsequent to completing two cycles between 250 and 700 °C.

Initially, the hydrogen permeability of the Pd membrane was determined in order to establish a reference with which to compare the performance of Membranes A–D as shown in Fig. 5. The temperature dependence of hydrogen permeability (Φ) in dense

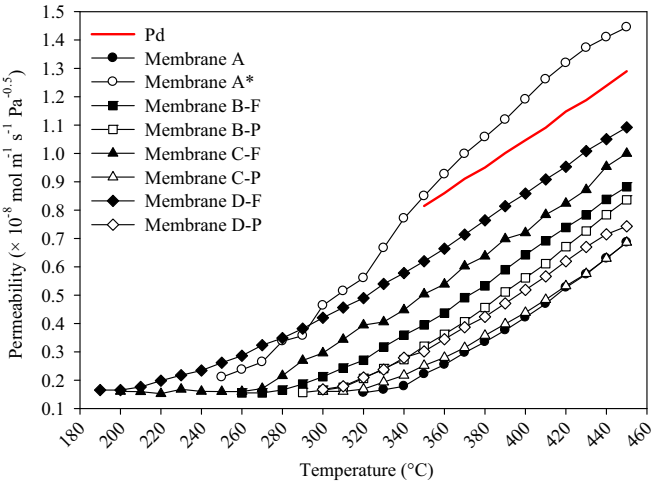

Fig. 5. Hydrogen permeability as a function of temperature plot comparing each membrane investigated in this work. All curves, except Membrane A*, show the heating stage of the initial third cycle completed by each membrane between 50 and 450 °C using a hydrogen feed pressure of 445 kPa and permeate pressure of 100 kPa. The Membrane A* curve represents the third cycle completed between 250 and 450 °C following the completion of two cycles between 250 and 700 °C.

metal membranes can be described using an Arrhenius type relationship:

$$\Phi = \Phi_0 \exp\left(\frac{-E_\Phi}{RT}\right) \quad (2)$$

where Φ_0 is the permeability constant, E_Φ is the activation energy for hydrogen permeation, R is the gas constant and T is the absolute temperature. The Φ_0 and E_Φ values for each membrane are compiled in Table 3, which have been determined between 350 and 450 °C from a plot of $\ln(\Phi)$ against reciprocal temperature, T^{-1}, using the data shown in Fig. 5.

The Φ_0 and E_Φ values determined for the bulk Pd membrane used in this work fall within the range found in literature which vary between $1.42–3.80 \times 10^{-7}$ mol m^{-1} s^{-1} Pa$^{-0.5}$ and 11.91–20.50 kJ mol^{-1} for Φ_0 and E_Φ, respectively [51–57], thus validating the hydrogen permeability measurements made using the MPR. Therefore, the permeability data obtained for the other membranes investigated in this work can be compared to those found in literature with high confidence.

The Φ_0 and E_Φ values for $Pd_{60}Cu_{40}$ wt% foil membranes are not available in literature; however, various authors [8,15,16,58–60] have reported hydrogen permeability values for this composition at 350 °C that range between 0.35 and 1.76×10^{-8} mol m^{-1} s^{-1} Pa$^{-0.5}$. At 350 °C, Membrane A achieves a hydrogen permeability of 2.21×10^{-9} mol m^{-1} s^{-1} Pa$^{-0.5}$ which falls below the literature range and as shown in Fig. 5 this membrane exhibits the lowest hydrogen permeability of all the membranes investigated in this work.

Interestingly, cycling Membrane A between 250 and 700 °C increases the hydrogen permeability by nearly a factor of four to 8.49×10^{-9} mol m^{-1} s^{-1} Pa$^{-0.5}$ at 350 °C as demonstrated by the Membrane A* curve in Fig. 5. It is apparent that homogenising Membrane A at relatively higher temperatures in a hydrogen atmosphere has the effect of reducing the Φ_0 by an order of magnitude, more than halving the E_Φ value and decreasing the hydrogen permeation start temperature from 300 to 250 °C.

For a fair assessment of the surface modified Pd–Cu membranes, comparisons will be drawn between Membranes A, B-F, B-P, C-F, C-P, D-F and D-P since these membranes completed the same number of cycles between 50 and 450 °C. Membranes B-F, B-P, C-F, C-P, D-F and D-P all exhibit improved hydrogen permeability in comparison to Membrane A. The data shown in Table 3 indicates that depositing Pd on to the surface of an as-received Pd–Cu foil membrane has the effect of increasing Φ_0 and decreasing E_Φ.

It is evident from Fig. 5, that positioning the Pd thin film on the permeate side during MPR testing improves hydrogen permeability of the membrane. Moreover, it is apparent that Membrane D-F, which was coated with the largest Pd thin film thickness (~1400 nm), achieves the highest hydrogen permeability of the surface modified membranes. Membrane C-F which was coated with an ~800 nm thick Pd thin film achieved the second highest hydrogen permeability of the surface modified Pd–Cu membranes followed by Membrane B-F which was coated with only a ~100 nm thick Pd thin film.

Positioning the Pd thin film of the surface modified membranes on the permeate side appears to reduce the value of Φ_0 and increase E_Φ resulting in a relatively lower hydrogen permeability in comparison to Membranes B-F, C-F and D-F. Membrane C-P has the lowest hydrogen permeability of the surface modified membranes. These findings are discussed in further detail in Section 3.4.

3.3. Post-MPR membrane characterisation

Following MPR testing, XRD analysis revealed that Membrane A contained only the ordered BCC equilibrium phase which had an average lattice parameter of 2.978 Å for both the feed and permeate side. These lattice parameters agree extremely well with the value range of 2.97–2.977 Å [14,26,42,61] found in literature for the same phase composition. Since the BCC crystal structure has a lattice parameter different from the FCC crystal structure, a new formula is required to accurately calculate the phase composition similar to Eq. (1). Using data compiled from literature [25–28,30,34–36,40], the following Eq. (3) can be derived.

$$a = (1.57 \times 10^{-3}) x_{Pd} + 2.90 \quad (3)$$

Table 3
Summary of permeability data obtained for the membranes investigated in this study.

	Permeability constant, Φ_0 ($\times 10^{-7}$ mol m^{-1} s^{-1} Pa$^{-0.5}$)	Hydrogen permeation activation energy, E_Φ (kJ mol^{-1})	Hydrogen permeability at 450 °C as shown in Fig. 5 ($\times 10^{-8}$ mol m^{-1} s^{-1} Pa$^{-0.5}$)
Pd	2.41	17.54	1.29
Membrane A	88.13	41.67	0.69
Membrane A*	6.32	19.93	1.44
Membrane B-F	13.26	29.95	0.88
Membrane B-P	36.93	36.41	0.84
Membrane C-F	4.99	23.41	1.00
Membrane C-P	38.83	38.01	0.69
Membrane D-F	3.44	20.52	1.09
Membrane D-P	21.89	33.91	0.74

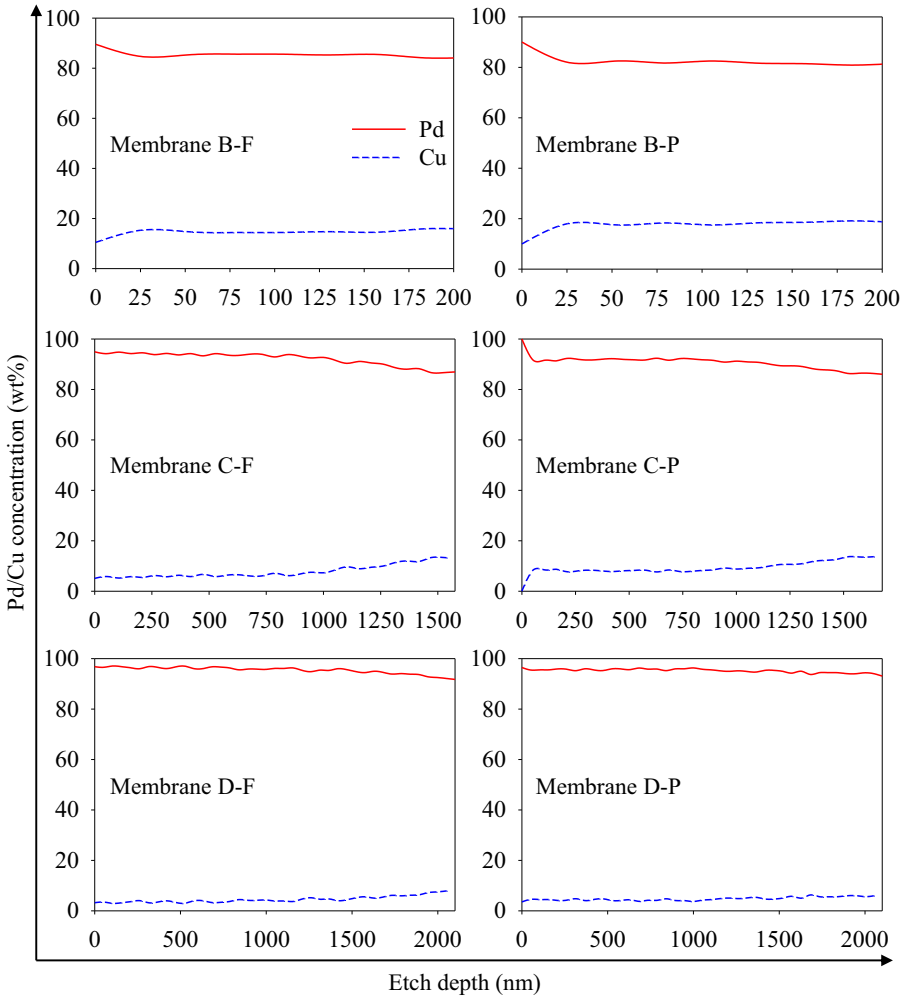

Fig. 6. XPS depth profile analysis of the Pd sputter coated surface of Membranes B-F, B-P, C-F, C-P, D-F and D-P following MPR testing.

Using Eq. (3), the Membrane A BCC phase composition can be calculated as $Pd_{61.6}Cu_{38.4}$ wt% for the feed and permeate side suggesting that a homogenous BCC phase was formed throughout the membrane as a result of the conditions used during MPR testing. The BCC phase composition was also determined with EDS analysis and agreed well with the compositions calculated using XRD analysis. Following MPR testing, EDS analysis revealed a composition of $Pd_{62.2\pm0.6}Cu_{37.8\pm0.6}$ wt% and $Pd_{61.9\pm0.9}Cu_{38.1\pm0.9}$ wt% for the feed side and permeate side of Membrane A, respectively. These compositions represent the homogenous ordered BCC phase and differ from the composition obtained for Membrane A Pre-MPR testing using EDS which is attributed to the inhomogeneous disordered FCC phase.

Fig. 6 shows results of the XPS depth profile analysis performed on the Pd sputter coated side of Membranes B-F, B-P, C-F, C-P, D-F and D-P after MPR testing revealing that interdiffusion has occurred between the Pd thin film and bulk Pd–Cu foil in each membrane. It is apparent that the interdiffusion region extends further beyond the analysis depth. Both XRD and XPS analyses indicate that completing three cycles between 50 and 450 °C under a hydrogen feed pressure of 445 kPa and permeate pressure of 100 kPa creates a Pd-rich Pd–Cu FCC phase on the Pd sputter coated side of the surface modified membranes. Table 4 shows the Pd thin film surface composition of the surface modified Pd–Cu membranes following MPR testing determined using XRD and XPS analysis. Both methods corroborate extremely well demonstrating that Membrane C-P retains a pure Pd surface after MPR testing.

3.4. Discussion of findings

The marked improvement in hydrogen permeability demonstrated by Membrane A can be attributed to the homogenisation of the membrane upon cycling up to 700 °C under conditions used during MPR testing.

Krueger [60] cites that homogenising an as-received $Pd_{60}Cu_{40}$ wt% foil membrane at 1100 °C in a mildly reducing atmosphere for 40 min can improve hydrogen permeability by up to 65%. Such an improvement has been linked to a phenomenon known as coring. This occurs when an alloy melt is cooled to the solid phase under non-equilibrium conditions causing the exterior of the alloy to solidify at a more rapid rate than the interior. The grains that form in the inner region are richer in the higher melting point component; in this case Pd, whereas the outer region grains will be Pd-depleted and so this effect will lead to compositional inhomogeneity within the alloy [60]. Such inhomogeneity can be of detriment to the performance of a Pd–Cu membrane since hydrogen permeability is sensitive to phase composition.

In addition to the effects of coring, Piper [14] stated that annealing at 350 °C in 507 kPa of hydrogen pressure can improve the room temperature diffusivity of a $Pd_{60}Cu_{40}$ wt% membrane by more than a factor of two over annealing under a vacuum at the same temperature. In general, annealing in a hydrogen atmosphere is beneficial for the membrane to reverse the effects of coring and promote the formation of the equilibrium BCC phase. It has been theorised that rapid phase transformation can occur in

Table 4
Composition of the Pd sputter coated surface of Membranes B-F, B-P, C-F, C-P, D-F and D-P following MPR testing determined using XRD and XPS analyses.

	Pd thin film surface composition post MPR testing (wt%) – XRD	Pd thin film surface composition post MPR testing (wt%) – XPS
Membrane B-F	$Pd_{83.6}Cu_{16.4}$	$Pd_{83.0}Cu_{17.0}$
Membrane B-P	$Pd_{83.0}Cu_{17.0}$	$Pd_{90.0}Cu_{10.0}$
Membrane C-F	$Pd_{97.0}Cu_{3.0}$	$Pd_{95.0}Cu_{5.0}$
Membrane C-P	$Pd_{100.0}Cu_{0.0}$	$Pd_{100.0}Cu_{0.0}$
Membrane D-F	$Pd_{98.8}Cu_{1.2}$	$Pd_{96.8}Cu_{3.2}$
Membrane D-P	$Pd_{99.9}Cu_{0.1}$	$Pd_{96.5}Cu_{3.5}$

the presence of hydrogen due to accelerated atomic diffusion and rearrangement caused by the formation of vacancy-hydrogen clusters [62–65] which is the trapping of hydrogen atoms in metal vacancies.

Fig. 5 and Table 3 indicate that depositing a Pd thin film onto one side of a $Pd_{60}Cu_{40}$ wt% foil membrane enhances hydrogen permeability by decreasing Φ_0 and increasing E_Φ. As evidenced by the XPS data shown in Fig. 6, the Pd thin film interdiffuses with the bulk Pd–Cu foil membrane during MPR testing to produce a compositional gradient on the Pd sputter coated surface. Fig. 7 shows that at room temperature the hydrogen to metal ratio (H/M) also referred to as the hydrogen solubility increases in a Pd–Cu alloy with increasing Pd content. Solubility data for the Pd–Cu system at higher temperatures is not available in literature although it is known that hydrogen solubility decreases in a Pd–Cu alloy with increasing temperature [38,66].

The solubility of hydrogen in a dense metal membrane can be described using Sieverts' law (Eq. (4)), where S is the solubility constant, C is the hydrogen concentration in the metal and P is the partial pressure of hydrogen in the gas phase.

$$S = \frac{C}{P^{\frac{1}{2}}} \tag{4}$$

Furthermore, hydrogen diffusion in a dense metal membrane can be modelled using Fick's first law (Eq. (5)) where J is hydrogen flux, D is the diffusion coefficient and x denotes the membrane thickness.

$$J = -D\frac{\partial C}{\partial x} \tag{5}$$

It follows that if the Pd thin film introduces a compositional gradient during MPR testing, this will in turn produce a hydrogen solubility gradient and therefore a hydrogen concentration gradient ($\partial C/\partial x$). According to Fick's first law (Eq. (5)), for a given temperature a concentration gradient is the driving force for hydrogen diffusion in a dense metal membrane and consequently hydrogen permeability.

Fig. 8(a) is a schematic representation of Membrane A during MPR testing which assumes a relatively uniform composition and Pd concentration throughout the membrane thickness. Applying a hydrogen pressure differential across the membrane creates the hydrogen concentration gradient necessary for conventional hydrogen diffusion.

Fig. 8(b) is a representation of Membranes B-F, C-F and D-F during MPR testing. Interdiffusion of the Pd thin film with the bulk Pd–Cu membrane during MPR testing creates a Pd concentration gradient and produces a Pd-rich Pd–Cu FCC phase on the Pd sputter coated surface of the membrane. This newly formed phase positioned on the feed side during MPR testing possesses a relatively higher hydrogen solubility thus introducing a much steeper hydrogen concentration gradient which could be responsible for the observed increase in hydrogen permeability.

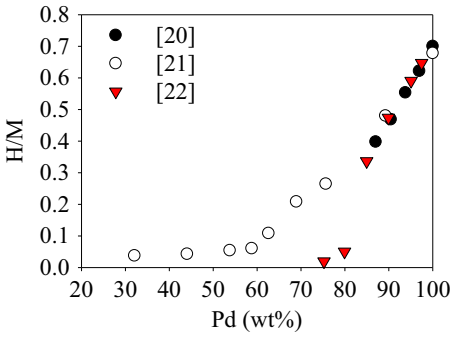

Fig. 7. Hydrogen solubility data for Pd–Cu alloys at room temperature and 101.325 kPa compiled from literature [20–22].

Comparing Membranes B-F, C-F and D-F, Membrane D-F has the highest hydrogen permeability, followed by Membrane C-F and lastly Membrane B-F. This is perhaps attributed to the thicker Pd thin film in Membrane D-F producing a surface with a relatively higher Pd concentration which increases hydrogen solubility and introduces a larger hydrogen concentration gradient responsible for the increase in hydrogen permeability.

Fig. 8(c) illustrates Membranes B-P, C-P and D-P during MPR testing. These membranes achieve a relatively higher hydrogen permeability than Membrane A yet a lower hydrogen permeability compared to Membranes B-F, C-F and D-F. The applied pressure differential produces the concentration gradient necessary for hydrogen permeation, however, the high hydrogen solubility of the Pd-rich Pd–Cu FCC phase on the permeate side likely creates a plateau in the concentration profile causing the slight reduction in hydrogen permeability. Membrane C-P achieves the lowest hydrogen permeability of all the surface modified membranes. This is possibly due to Membrane C-P forming a pure Pd surface on the Pd sputter coated side during MPR testing which produces a larger plateau in the concentration profile resulting in the observed decrease in hydrogen permeability.

The Pd membrane used in this work was never cycled below the critical temperature (295 °C) during MPR testing in order to avoid the phase transformation from the interstitial hydrogen solid solution phase to the Pd-hydride phase, which involves a lattice volume expansion capable of causing membrane failure. However, it has been observed that the membranes that maintain a relatively pure Pd surface during MPR testing (Membranes C-F, C-P, D-F and D-P) are capable of being cycled to temperatures as low as 50 °C without showing any evidence of film delamination or membrane failure. The bulk Pd–Cu membrane substrate appears to stabilise the Pd thin film below the critical temperature, which prevents delamination under the conditions used during MPR testing.

4. Conclusions

For the first time, the hydrogen permeability of surface modified $Pd_{60}Cu_{40}$ wt% membranes have successfully been measured in this work. For a valid assessment, membranes which have completed the same number of cycles under the same test conditions in the MPR system are compared.

The hydrogen permeability was measured for Membrane A in the as-received state by cycling between 50 and 450 °C. On the third cycle, the hydrogen permeability for Membrane A at 450 °C was 6.86×10^{-9} mol m^{-1} s^{-1} $Pa^{-0.5}$ which is relatively low compared with published data. However, it was found that cycling Membrane A to temperatures as high as 700 °C, had the effect of

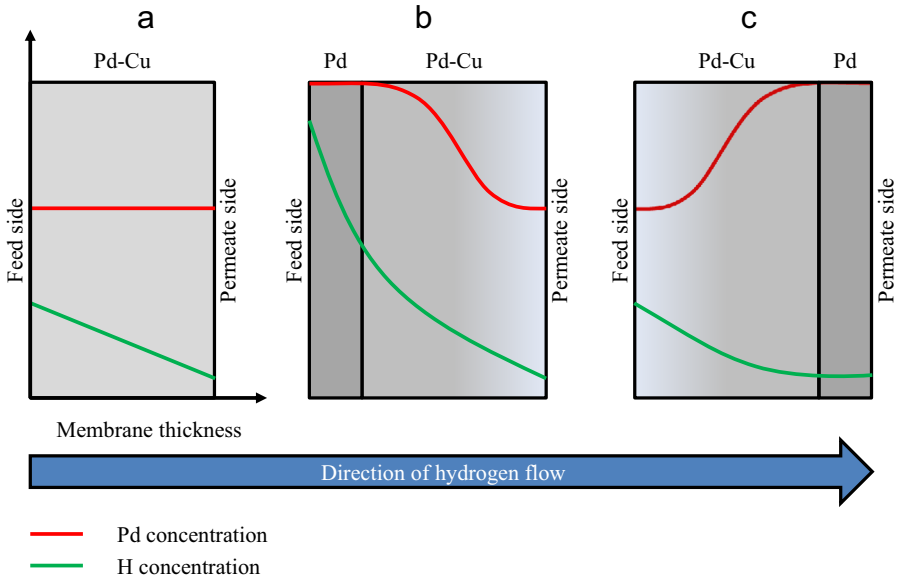

Fig. 8. A schematic illustration showing Pd and H concentration as a function of membrane thickness during MPR testing at a given temperature where (a) represents Membrane A, (b) represents Membranes B-F, C-F and D-F; and (c) represents Membranes B-P, C-P and D-P.

reducing the E_{Φ} value by a factor of two resulting in a hydrogen permeability at 450 °C of 1.44×10^{-8} mol m^{-1} s^{-1} Pa$^{-0.5}$. This new value is in good agreement with the published figures [15,16,59].

Coring was discovered to be responsible for the initially low hydrogen permeability value demonstrated by Membrane A. Coring likely occurred as a result of rapid cooling of the Pd–Cu alloy melt thus retaining the high temperature disordered FCC phase down to room temperature as shown using XRD analysis. Furthermore, this created compositional inhomogeneity as the component with the lowest melting point, in this case Cu atoms, solidifies first and migrates to the outer extremities of the alloy leaving the Pd atoms to concentrate in the inner regions.

Prolonged cycling and exposure to elevated temperatures in hydrogen was found to be effective in homogenising Membrane A and increasing its hydrogen permeability. Krueger [60] reports a similar observation with a Pd–Cu alloy membrane and proposes that annealing at temperatures close to the melting point of Cu in an atmosphere containing hydrogen is sufficient to reverse the effects of coring and significantly enhance hydrogen permeability.

The surface modified membranes achieved a relatively higher hydrogen permeability at 450 °C during the initial third cycle in comparison to Membrane A at the corresponding temperature and cycle. During MPR testing, XPS analysis showed interdiffusion between the Pd thin film and the bulk Pd–Cu membrane form both a Pd-rich Pd–Cu FCC phase and a compositional gradient on the Pd sputter coated side of the surface modified membranes. Positioning the Pd sputter coated side of the surface modified membranes on the feed side during MPR testing creates a larger than normal concentration gradient due to the higher hydrogen solubility of the Pd-rich Pd–Cu FCC phase. This increased hydrogen concentration gradient is likely the cause of the relatively higher hydrogen permeability displayed by Membranes B-F, C-F and D-F.

In contrast, positioning the Pd sputter coated side of the surface modified Pd–Cu membranes on the permeate side during MPR testing may have the opposite effect. The pressure differential across the membrane creates the concentration gradient necessary for permeation, although the Pd-rich Pd–Cu FCC phase positioned on the permeate side introduces a hydrogen solubility gradient acting in the direction opposing hydrogen diffusion. This may have the effect of producing a plateau in the hydrogen concentration profile towards the permeate side of the membrane hence reducing the hydrogen permeability in Membranes B-P, C-P and D-P.

Furthermore, it was discovered that Membranes C-F, C-P, D-F and D-P retained an almost pure Pd surface following MPR testing and showed no signs of film delamination or disintegration as result of cycling between 50 and 450 °C in a hydrogen atmosphere.

Given reports of the Pd-rich Pd–Cu FCC phase exhibiting greater resistance to H_2S contamination compared to the Pd–Cu BCC phase [10,11,59], the surface modified Pd–Cu membranes investigated in this work may have potential to separate hydrogen from a gas mixture containing H_2S under typical membrane operating conditions with improved durability.

Acknowledgements

The authors are grateful to Johnson Matthey Noble Metals (Royston, UK) for the provision of rolled Pd–Cu foils, and to NEXUS nanoLab (Newcastle University) for performing the XPS analysis. Support from the EPSRC, United Kingdom DTC in Hydrogen, Fuel Cells and their Applications (EP/G037116/1) is gratefully acknowledged.

References

[1] L. Barelli, G. Bidini, F. Gallorini, S. Servili, Hydrogen production through sorption-enhanced steam methane reforming and membrane technology: a review, Energy 33 (2008) 554–570.
[2] J.D. Holladay, J. Hu, D.L. King, Y. Wang, An overview of hydrogen production technologies, Catal. Today 139 (2009) 244–260.
[3] A. Faur Ghenciu, Review of fuel processing catalysts for hydrogen production in PEM fuel cell systems, Curr. Opin. Solid State Mater. Sci. 6 (2002) 389–399.
[4] A.G. Knapton, Palladium alloys for hydrogen diffusion membranes, Platin. Met. Rev. 21 (1977) 44–50.
[5] S. Adhikari, S. Fernando, Hydrogen membrane separation techniques, Ind. Eng. Chem. Res. 45 (2006) 875–881.
[6] S.N. Paglieri, J.D. Way, Innovations in palladium membrane research, Sep. Purif. Methods 31 (2002) 1–169.
[7] D.L. McKinley, Metal alloy for hydrogen separation and purification, U.S. Patent 3,350,845, 1967.
[8] D.L. McKinley, Method for hydrogen separation and purification, U.S. Patent 3,439,474, 1969.
[9] K.S. Rotherberg, B.H. Howard, R.P. Killmeyer, M.V. Ciocco, B.D. Morreale, R. M. Enick, Palladium–copper alloy membrane performance under continuous exposure, National Hydrogen Association, Washington, DC (2005), p. 1–10.

[10] N. Pomerantz, Y.H. Ma, Effect of H_2S on the performance and long-term stability of Pd/Cu membranes, Ind. Eng. Chem. Res. 48 (2009) 4030–4039.
[11] N. Pomerantz, Y.H. Ma, Novel method for producing high H_2 permeability Pd membranes with a thin layer of the sulfur tolerant Pd/Cu fcc phase, J. Membr. Sci. 370 (2011) 97–108.
[12] B. Morreale, M. Ciocco, B. Howard, R. Killmeyer, A. Cugini, R. Enick, Effect of hydrogen-sulfide on the hydrogen permeance of palladium–copper alloys at elevated temperatures, J. Membr. Sci. 241 (2004) 219–224.
[13] P. Subramanian, D. Laughlin, Cu–Pd (copper–palladium), J. Phase Equilib. 12 (1991) 231–243.
[14] J. Piper, Diffusion of hydrogen in copper–palladium alloys, J. Appl. Phys. 37 (1966) 715–721.
[15] B. Howard, R. Killmeyer, K. Rothenberger, A. Cugini, B. Morreale, R. Enick, F. Bustamante, Hydrogen permeance of palladium–copper alloy membranes over a wide range of temperatures and pressures, J. Membr. Sci. 241 (2004) 207–218.
[16] L. Yuan, A. Goldbach, H. Xu, Permeation hysteresis in PdCu membranes, J. Phys. Chem. B 112 (2008) 12692–12695.
[17] M. Li, Z. Du, C. Guo, C. Li, A thermodynamic modeling of the Cu–Pd system, Calphad 32 (2008) 439–446.
[18] J. Völkl, G. Alefeld, Diffusion of hydrogen in metals, in: G. Alefeld, J. Völkl (Eds.), Hydrogen in Metals I, Springer, Berlin, 1978, pp. 321–348.
[19] P. Kamakoti, D.S. Sholl, A comparison of hydrogen diffusivities in Pd and CuPd alloys using density functional theory, J. Membr. Sci. 225 (2003) 145–154.
[20] M.H. Martin, J. Galipaud, A. Tranchot, L. Roué, D. Guay, Measurements of hydrogen solubility in Cu_xPd_{100-x} thin films, Electrochim. Acta 90 (2012) 615–622.
[21] T. Flanagan, D. Chisdes, Solubility of hydrogen (1 atm, 298 K) in some copper/palladium alloys, Solid State Commun. 16 (1975) 529–532.
[22] R. Burch, R. Buss, Absorption of hydrogen by palladium–copper alloys – theoretical analysis, J. Chem. Soc. Faraday Trans. 1: Phys. Chem. Condens. Phases 71 (1975) 922–929.
[23] K. Cooke, J. Hamsphire, W. Southall, D. Teer, The industrial application of pulsed DC bias power supplies in closed field unbalanced magnetron sputter ion plating, Surf. Coat. Technol. 177 (2004) 789–794.
[24] L. Vegard, Die konstitution der mischkristalle und die raumfüllung der atome, Z. Physik A Hadron. Nucl. 5 (1921) 17–26.
[25] S. Holgersson, E. Sedstrom, Experimental investigation on the lattice structure of certain metallic alloys, Ann. Phys. 75 (1924) 143–162.
[26] J.O. Linde, The lattice constants of Cu–Pd binary alloys, Ann. Phys. 15 (1932) 249–251.
[27] L. Graf, Kinetics and mechanism of transformation in the system palladium–copper (X-ray investigation of single crystals with 40–50 at% Pd), Z. Phys. A Hadron. Nucl. 36 (1935) 489–498.
[28] F.W. Jones, C. Sykes, The transformations in the copper-palladium alloys, J. Inst. Met. 65 (1939) 419–433.
[29] A.H. Geisler, J.B. Newkirk, Ordering reaction of the Cu_4Pd alloy, Trans. Am. Insti. Min. Metall. Pet. Eng., 200, (1954) 1076–1082.
[30] K. Schubert, B. Kiefer, M. Wilkens, R. Haufler, On some metallic ordered phases with long periods, Z. Met. 46 (1955) 692–715.
[31] F. Jaumot, A. Sawatzky, An isothermal anneal study of quenched and cold-worked copper–palladium alloys, Acta Metall. 4 (1956) 118–126.
[32] M. Hirabayashi, S. Ogawa, On the superstructure of the ordered alloy Cu_3Pd. II. X-ray diffraction study, J. Phys. Soc. Jpn. 12 (1957) 259–271.
[33] A.A. Presnyakov, A.A. Karpenyuk, E.A. Dzhanbusinov, Features of the ordering of a dilute solid solution of palladium in copper, Trudy Inst. Yad. Fiz. Nauk Kaz. SSR 10 (1969) 45–51.
[34] E. Raub, O.L. Jr., W. Plate, H. Krill, The structure of ternary copper–nickel–palladium alloys between temperatures of 400 to 700 °C, Z. Met. 62 (1971) 826–830.
[35] V.V. Sanadze, M.V. Dzhibuti, Disordering process in a Cu–Pd alloy, Trudy Gruz. Politekh. Inst. 6 (1972) 70–75.
[36] K. Imakuma, Phase transformations in $Cu_{0.6}Pd_{0.4}$ alloy, Instituto de Energia Atomica, 1978.
[37] T.B. Massalski, H. Okamoto, P. Subramanian, L. Kacprzak, Binary Alloy Phase Diagrams, ASM International, Materials Park, OH, 1990.
[38] R. Burch, R. Buss, Absorption of hydrogen by palladium–copper alloys – experimental measurements, J. Chem. Soc. Faraday Trans. 1: Phys. Chem. Condens. Phases 71 (1975) 913–921.
[39] S. Nayebossadri, J. Speight, D. Book, Effects of low Ag additions on the hydrogen permeability of Pd–Cu–Ag hydrogen separation membranes, J. Membr. Sci. 451 (2014) 216–225.
[40] L. Yuan, A. Goldbach, H. Xu, Segregation and H_2 transport rate control in body-centered cubic PdCu membranes, J. Phys. Chem. B 111 (2007) 10952–10958.
[41] P.L. Gai, B.C. Smith, Dynamic electron microscopy of copper-palladium intermetallic compound catalysts, Ultramicroscopy 34 (1990) 17–26.
[42] H. Gao, J.Y.S. Lin, Y. Li, B. Zhang, Electroless plating synthesis, characterization and permeation properties of Pd–Cu membranes supported on ZrO_2 modified porous stainless steel, J. Membr. Sci. 265 (2005) 142–152.
[43] F. Roa, J.D. Way, The effect of air exposure on palladium–copper composite membranes, Appl. Surf. Sci. 240 (2005) 85–104.
[44] R. Merkle, J. Maier, On the Tammann – Rule, Z. Anorg. Allg. Chem. 631 (2005) 1163–1166.
[45] S. Nakahara, J.A. Abys, S.M. Abys, Room-temperature diffusion-induced grain boundary migration in the fine-grained Pd side of Cu–Pd diffusion couples, Mater. Lett. 2 (1983) 155–159.
[46] Y. Kuru, M. Wohlschlögel, U. Welzel, E.J. Mittemeijer, Interdiffusion and stress development in Cu–Pd thin film diffusion couples, Thin Solid Films 516 (2008) 7615–7626.
[47] J. Chakraborty, U. Welzel, E. Mittemeijer, Mechanisms of interdiffusion in Pd–Cu thin film diffusion couples, Thin Solid Films 518 (2010).
[48] J. Chakraborty, U. Welzel, E. Mittemeijer, Interdiffusion, phase formation, and stress development in Cu–Pd thin-film diffusion couples: Interface thermodynamics and mechanisms, J. Appl. Phys. 103 (2008) 113512.
[49] A. Bukaluk, Influence of depth resolution on interdiffusion measurements in polycrystalline Cu/Pd multilayers, Surf. Interface Anal. 30 (2000) 597–602.
[50] A. Bukaluk, AES studies of interdiffusion in thin-film copper–palladium multilayer structures, Vacuum 54 (1999) 279–283.
[51] S. Fletcher, Thin film palladium–yttrium membranes for hydrogen separation (Ph.D thesis), University of Birmingham, 2009.
[52] G.L. Holleck, Diffusion and solubility of hydrogen in palladium and palladium-silver alloys, J. Phys. Chem. 74 (1970) 503–511.
[53] R. Hurlbert, J. Konecny, Diffusion of hydrogen through palladium, J. Chem. Phys. 34 (1961) 655–658.
[54] H. Katsuta, R. Farraro, R. McLellan, The diffusivity of hydrogen in palladium, Acta Metall. 27 (1979) 1111–1114.
[55] S.A. Koffler, J.B. Hudson, G.S. Ansell, Hydrogen permeation through alpha-palladium, Trans. Metall. Soc. Am. Inst. Min. Metall. Pet. Eng. 245 (1969) 1735–1740.
[56] B.D. Morreale, M.V. Ciocco, R.M. Enick, B.I. Morsi, B.H. Howard, A.V. Cugini, K. S. Rothenberger, The permeability of hydrogen in bulk palladium at elevated temperatures and pressures, J. Membr. Sci. 212 (2003) 87–97.
[57] G. Toda, Rate of permeation and diffusion coefficient of hydrogen through palladium, J. Res. Inst. Catal. Hokkaido Univ. 6 (1958) 13–19.
[58] C. Decaux, R. Ngameni, D. Solas, S. Grigoriev, P. Millet, Time and frequency domain analysis of hydrogen permeation across PdCu metallic membranes for hydrogen purification, Int. J. Hydrog. Energy 35 (2010) 4883–4892.
[59] P. Kamakoti, B.D. Morreale, M.V. Ciocco, B.H. Howard, R.P. Killmeyer, A. V. Cugini, D.S. Sholl, Prediction of hydrogen flux through sulfur-tolerant binary alloy membranes, Science 307 (2005) 569–573.
[60] C. Krueger, Method of improving and optimizing the hydrogen permeability of a palladium–copper membrane and novel membranes manufactured thereby, U.S. Patent 6,372,363 B1, 2002.
[61] F. Roa, J.D. Way, Influence of alloy composition and membrane fabrication on the pressure dependence of the hydrogen flux of palladium-copper membranes, Ind. Eng. Chem. Res. 42 (2003) 5827–5835.
[62] E. Hayashi, Y. Kurokawa, Y. Fukai, Hydrogen-induced enhancement of interdiffusion in Cu–Ni diffusion couples, Phys. Rev. Lett. 80 (1998) 5588–5590.
[63] N. Fukumuro, M. Yokota, S. Yae, H. Matsuda, Y. Fukai, Hydrogen-induced enhancement of atomic diffusion in electrodeposited Pd films, J. Alloy. Compd. 580 (Suppl. 1) (2013) S55–S57.
[64] T.B. Flanagan, C.-N. Park, Hydrogen-induced rearrangements in Pd-rich alloys, J. Alloy. Compd. 293 (1999) 161–168.
[65] Y. Fukai, Formation of superabundant vacancies in M–H alloys and some of its consequences: a review, J. Alloy. Compd. 356 (2003) 263–269.
[66] R. Burch, R. Buss, Pressure-composition isotherms in the palladium–copper–hydrogen system, Solid State Commun. 15 (1974) 407–409.